Phase Diagram of a Three-Dimensional Antiferromagnet with Random Magnetic Anisotropy

Felio A. Perez, Pavel Borisov, Trent A. Johnson, Tudor D. Stanescu, Robbyn Trappen, Mikel B. Holcomb, David Lederman, M. R. Fitzsimmons, Adam A. Aczel, and Tao Hong

Phys. Rev. Lett. **114**, 097201 — Published 4 March 2015

DOI: 10.1103/PhysRevLett.114.097201

Phase diagram of a three-dimensional antiferromagnet with random magnetic anisotropy

Felio A. Perez,* Pavel Borisov, Trent A. Johnson, Tudor D. Stanescu,
Robbyn Trappen, Mikel B. Holcomb, and David Lederman†
Department of Physics and Astronomy,
West Virginia University, Morgantown, WV 26506-6315, USA

M. R. Fitzsimmons
Los Alamos National Laboratory, Los Alamos, NM 87545, USA

Adam A. Aczel and Tao Hong
Quantum Condensed Matter Division,
Oak Ridge National Laboratory, Oak Ridge, TN 37831, USA

(Dated: February 23, 2015)

Abstract

Three-dimensional (3D) antiferromagnets with random magnetic anisotropy (RMA) that have been experimentally studied to date have competing two-dimensional and three-dimensional exchange interactions which can obscure the authentic effects of RMA. The magnetic phase diagram of $Fe_xNi_{1-x}F_2$ epitaxial thin films with true random single-ion anisotropy was deduced from magnetometry and neutron scattering measurements and analyzed using mean field theory. Regions with uniaxial, oblique and easy plane anisotropies were identified. A RMA-induced glass region was discovered where a Griffiths-like breakdown of long-range spin order occurs.

PACS numbers: 75.30.Kz, 75.50.Ee, 75.10.Hk, 75.70.-i, 71.23.-k

There is much interest in understanding the properties of random magnets because of possible applications in magnetic recording technology, such as modulating exchange bias using antiferromagnets (AFs) with magnetic disorder [1, 2], and because their behavior can be used to understand complex systems in general [3–5]. For example, new quantum computing algorithms use quantum annealing protocols developed to probe spin glasses [6], social networks can be modeled via competing interactions between nodes [7–9], and random magnet models can be applied to protein folding and protein aggregation dynamics [10–12]. Antiferromagnetic alloys with magnetic disorder exhibit a wide range of complex phenomena described by spin glass, random exchange, random anisotropy, and random field Ising models [13] and are thus experimental realizations [14, 15] of theoretical models that describe random magnets [16–18]. Therefore, understanding the behavior of random magnets can lead to insights about the nature of complexity resulting from random interactions.

Here we focus on AFs with single site random magnetic anisotropy (RMA). Antiferromagnetic alloys, such as $Fe_xCo_{1-x}Cl_2$, $Fe_xCo_{1-x}Br_2$, $Fe_xCo_{1-x}TiO_3$, and $K_2Co_xFe_{1-x}F_4$, have been studied previously in which the effective RMA (ERMA) consists of competing intra- and inter-layer magnetic exchange coupling constants [14, 15, 19–24]. However, competing exchange interactions do not map to a single-site magnetic anisotropy near the phase transition temperature, and therefore the critical behavior of these systems is not representative of a true AF with RMA. This can be demonstrated using the spin Hamiltonian

$$H = \Sigma_i D \left(S_i^z\right)^2 + \Sigma_{ij} \Delta J_{ij} S_i^z S_j^z + \Sigma_{ij} J_{ij} \mathbf{S}_i \cdot \mathbf{S}_j, \tag{1}$$

where $\mathbf{S}_i$ is the spin vector at the i^{th} site, D is a single-site anisotropy constant, ΔJ_{ij} is the difference between intra- and inter-layer exchange coupling constants, and J_{ij} is the intra-layer exchange coupling constant. In the mean field approximation, taking into account only strongest neighbor interactions J, the Hamiltonian for a spin on the λ sublattice of the AF becomes

$$H_\lambda = D \left(S_\lambda^z\right)^2 + z \Delta J S_\lambda^z \left\langle S_{\overline{\lambda}}^z \right\rangle + z J \mathbf{S}_\lambda \cdot \langle \mathbf{S}_{\overline{\lambda}} \rangle \,, \tag{2}$$

where z is the number of neighbors located on the sublattice $\overline{\lambda}$ that interact with a spin $\mathbf{S}_\lambda$. The second term on the right hand side of Eq. 2, the effective single-ion magnetic anisotropy resulting from the anisotropic exchange interaction, is strongly temperature (T) dependent near the Néel temperature T_N because $\langle S_i^z \rangle \to 0$ as $T \to T_N$. On the other hand, the first term, which represents a true single-ion anisotropy, is not T dependent and therefore domi-

nates the physics in the vicinity of the magnetic phase transition. Consequently, the physics that governs a system with true random single-ion anisotropy near the phase transition will be in general different from the physics generated by an ERMA produced by anisotropic exchange interactions. Specifically, the effects of spin fluctuations resulting from the RMA will be masked for $T \sim T_N$ for the ERMA model, while they should dominate for the true RMA model (this is the same reason why a non-random system with $D < 0$, such as FeF_2, behaves like an ideal Ising model for $T \sim T_N$ [25]). Moreover, renormalization group theory calculations indicate that the type of magnetic disorder (e.g., random infinite-component anisotropy, two-component random anisotropy, competing random exchange interactions) have significant effects on the phase diagram and phase transition phenomena [26]. Here we report on the phase diagram of a solid solution of two 3D AFs that have random orthogonal anisotropies originating solely from the single-ion anisotropies of each component. We observe a RMA-induced glassy region near T_N which results from the strong RMA present in this system.

FeF_2 and NiF_2 share the rutile crystal structure with similar lattice parameters ($a = b = 4.6974$ Å, $c = 3.3082$ Å for FeF_2 and $a = b = 4.6501$ Å, $c = 3.0835$ Å for NiF_2 at $T = 290$ K) [27, 28]. Both materials are 3D AFs with similar exchange interaction strengths with similar T_Ns, 73.2K and 78.4K, for NiF_2 and FeF_2, respectively [25, 29]. Their magnetic anisotropies are, however, very different. FeF_2 has a strong uniaxial anisotropy which results in its magnetic moments being aligned along the tetragonal c-axis [25]. In NiF_2, moments order antiferromagnetically in the $a-b$ plane (Fig. 1) and are canted by $\approx 0.4^\circ$ with respect to the a- or b-axis [29]. Weak ferromagnetism in NiF_2 is due to the presence of two non-equivalent magnetic sites in the NiF_2 crystal lattice [30]. The similarity of crystal structures and magnetic exchange interactions in NiF_2 and FeF_2 suggests that $Fe_xNi_{1-x}F_2$ is an ideal system to study RMA, where the anisotropy depends on whether a site is occupied by Ni^{2+} (favoring $a-b$ plane ordering) or Fe^{2+} (favoring c-axis ordering) [2, 31].

Epitaxial (110) $Fe_xNi_{1-x}F_2$ films were grown with nominal thicknesses of 37 and 100 nm on (110) MgF_2 substrates at 300 ^{o}C via molecular beam epitaxy [2, 32] and capped with 10 nm BaF_2 or Pd layers to prevent oxidation. The Fe concentration x was determined using a quartz-crystal monitor with an accuracy of ± 0.05 [2, 32]. X-ray diffraction indicated a systematic change in the lattice parameter with x, with no evidence of NiF_2/FeF_2 phase segregation and a structural domain size of approximately 20 nm [33]. X-ray photoelec-

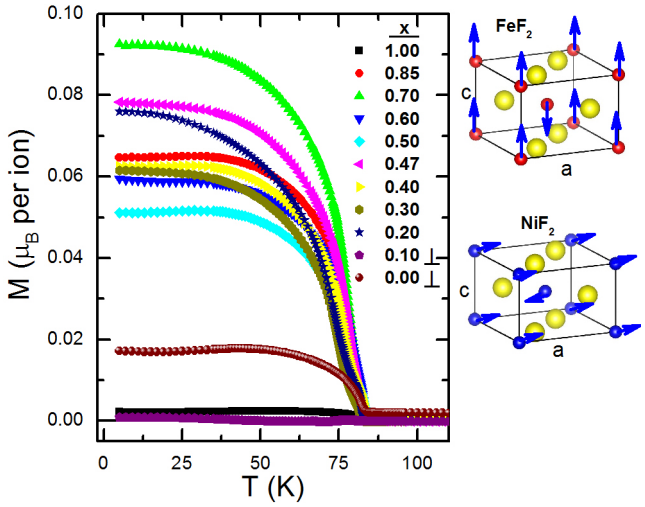

FIG. 1. TRM for $Fe_xNi_{1-x}F_2$ samples measured in $H = 0$ after field cooling in $H_{FC} = 100$ Oe. Data for $x = 0$ and 0.10 were measured with H_{FC} perpendicular to the c-axis; all others measured with H_{FC} parallel to the c-axis. Right: magnetic and crystalline structures of the parent compounds NiF_2 ($x = 0$) and FeF_2 ($x = 1$). Yellow, blue, and red dots are F^-, Ni^{2+} and Fe^{2+} ions, respectively.

tron and x-ray absorption spectroscopy (XPS and XAS), as well as x-ray magnetic circular dichroism (XMCD) measurements indicated that the local environment of the Fe and Ni ions was consistent with what is expected from the fluoride rutile structure and no impurities were detected [33].

Thermal remanent magnetization (TRM) measurements consisted of measuring the magnetization M while increasing T from $T = 5$ K in $H = 0$ after field-cooling (FC) from $T = 300$ K in a field $H_{FC} = 100$ Oe (Fig. 1) along the in-plane [001] (c-axis) and [1$\bar{1}$0] ($\perp$ c-axis) directions. The transition temperatures were determined by fitting the data near the phase transition with a rounded power-law

$$I = \frac{I_0}{\sigma_c\sqrt{2\pi}} \int_0^\infty (1 - T/T_c')^\beta \, e^{-(T_c - T_c')^2/2\sigma_c^2} dT_c', \tag{3}$$

where T_c is a transition temperature, β is a critical exponent, σ_c is the width of the transition, and I_0 is an overall scaling factor [34, 35]. Magnetic hysteresis loops were measured as a function of T and found to be in agreement with previous measurements of $Fe_xNi_{1-x}F_2$/Co bilayers [2, 32, 33]. FC and zero-field cooled (ZFC) measurements of M vs. T of all alloy samples behaved in a way that can be explained by the appearance of a ferromagnetic multi-domain state during the ZFC process and its realignment after field-cooling (see Fig. 2

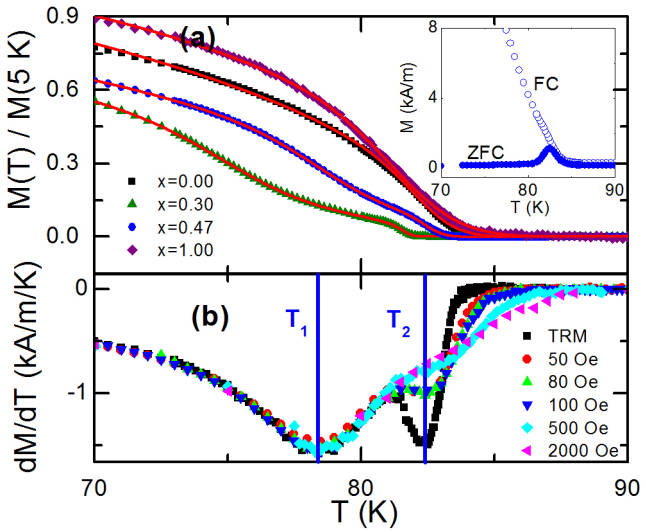

FIG. 2. (a) TRM data near the phase transition for four representative samples. Symbols are data and red curves are fits to Eq. 3 with two transitions for $x = 0.30, 0.47$ and one transition for $x = 1.0$ and $x = 0.0$. Inset: M measured while warming with $H = 80$ Oe applied along the c-axis after ZFC from $T = 300$ K to 5 K and during FC from 300 K to 5 K for the $x = 0.47$ sample. (b) $\partial M/\partial T$ of the $x = 0.47$ TRM and FC data measured under different applied fields. Vertical blue lines indicate transition temperatures T_1 and T_2.

inset). TRM data in Fig. 1 show the general effect of alloying on M. Small deviations of x from the pure phases resulted in significant increases of M at low T, but these values were much smaller than would be expected for ferrimagnetic order [36], and are therefore due to magnetic disorder.

TRM phase transitions with $H_{FC} \parallel$ c-axis, and $H_{FC} \perp$ c-axis for various samples are shown in Fig. 2(a). The TRM data for all alloy samples had an inflection at a lower T than the actual onset of the remanent magnetization, while the pure FeF_2 and NiF_2 samples only had one transition. The fits to the data using Eq. 3 with two transitions for the alloys and one transition for the pure samples, indicated that $\beta \approx 0.34 \pm 0.05$ for all samples. The presence of two phase transitions is more clear in the form of two minima at $T = T_1$ and T_2 by calculating $\partial M/\partial T$ vs. T, as shown in Fig. 2(b). When M was measured in a small H_{FC} applied along the c-axis, the transition at T_2 broadened substantially with respect to the TRM, while the transition at T_1 and the low T behavior remained unaffected. This occurred for all samples with $0.2 < x < 1.0$. For $x = 0.1$, a similar transition was observed

with $H \perp c$, indicating the existence of the easy-plane ordering similar to that of pure NiF_2; for $H \parallel c$, the data had unusual behavior [33] due to the existence of an oblique phase, as discussed below.

There are two possible explanations for the $T_1 < T < T_2$ behavior: (1) a first order spin-reorientation transition from an Ising-like, single-axis anisotropy structure, similar to FeF_2, to a weakly ferromagnetic structure, similar to NiF_2, at $T = T_1$ with increasing T, or (2) a transition at $T = T_1$ from the FeF_2 magnetic structure to a magnetically disordered structure. To determine which explanation is correct, neutron scattering was measured in $x = 0.1$ and $x = 0.3$ 100 nm thick samples [33]. Prior to measurement, the samples were cooled in $H_{FC} = 60$ Oe $\parallel$ c-axis. Once cooled to $T = 4$ K, H was removed and the integrated intensities of the magnetic (100) and (001) reflections with their background subtracted, $I_{(100)}$ and $I_{(001)}$, were measured as a function of increasing T. From neutron scattering selection rules, $I_{(100)} \propto L_{\rm c}^2 + L_{\rm b}^2$, where $L_{\rm b,c}$ is the component of the staggered magnetization vector $\mathbf{L}$ of the AF along the c- or b-axis, while $I_{(001)} \propto L_{\rm ab}^2$, where $L_{\rm ab}^2 = L_{\rm a}^2 + L_{\rm b}^2$ is the component of $\mathbf{L}$ in the $a - b$ plane. Here $\mathbf{L} = (\mathbf{M_1} - \mathbf{M_2})$, where $\mathbf{M_{1,2}}$ are the two sublattice magnetization vectors with $M_1 = M_2$. Explanation (1) would result in $I_{(001)} \neq 0$ only in the $T_1 < T < T_2$ temperature range. On the other hand, explanation (2) requires that $I_{(100)}, I_{(001)} > 0$ only for $T < T_1$ because lack of long-range order in the $T_1 < T < T_2$ range would preclude the observation of magnetic scattering. For both samples, the data in Fig. 3(a) indicated the presence of a single transition, and therefore explanation (2) must be correct.

For the $x = 0.3$ sample, $I_{(001)} = 0$ for $0 < T < 85$ K, and therefore the spins ordered along the c-axis only. Fitting the data to a rounded power law phase transition similar to Eq. 3, but with $\beta \to 2\beta$ because $I \propto L^2$, yielded the results shown in Fig. 3(b). The value of T_N coincided with T_1 measured for $x = 0.1$ and $x = 0.3$ samples within uncertainties. The values of β from neutron scattering agreed with those from the TRM measurements, which are in better agreement with critical exponents associated with 3D Ising, Heisenberg, and random exchange models ($\beta \approx 0.35$) [25] than with the 3D random field model ($\beta \sim 0.1$) [34, 37, 38].

For the $x = 0.1$ sample, both $I_{(100)}$ and $I_{(001)}$ were non-zero at low T, and both $\to 0$ as $T \to T_N$, which indicates that $\mathbf{L}$ pointed at an oblique angle θ between the c-axis and the a-b plane for $T < T_N$. The values of $\theta(T)$ were calculated using $\tan\theta = \left(I_{(001)}/I_{(100)} - 1/2\right)^{1/2}$, where $L^2 = L_c^2 + L_{ab}^2$ and assuming that $L_b = L_a$. The results are shown in Fig. 3(c).

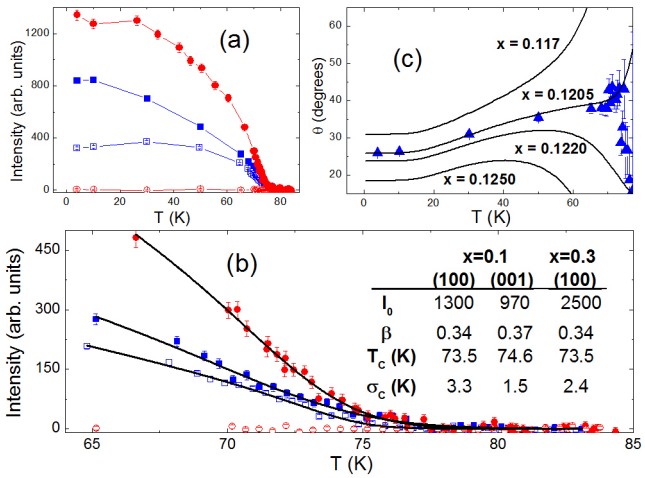

FIG. 3. (a) Neutron scattering intensity as a function of T for the $x = 0.3$ (red ◯) and $x = 0.1$ samples (blue □). Filled and open symbols indicate (100) and (001) reflections, respectively. Lines are guides to the eye. (b) Intensity near T_c. Black curves are best fits to Eq. 3 (with $\beta \to 2\beta$) with the parameters shown in the graph. (c) Angle of $\mathbf{L}$ as a function of T with respect to the c-axis for the $x = 0.1$ sample calculated from the data in (a). The solid curves are MFT results for the values of x indicated in the graph.

The phase diagram in Fig. 4, constructed from the TRM and neutron scattering data, can be modeled using mean field theory (MFT) [30, 33, 39]. MFT results are shown in Fig. 4. The paramagnet (PM)-AF phase transition boundary was reproduced by setting the exchange constants to $J_{\mathrm{FeFe}} = 0.475$ meV, $J_{\mathrm{NiNi}} = 1.63$ meV, and $J_{\mathrm{NiFe}} = 0.94$ meV, and using the known single-ion anisotropy constants $D_{Fe} = -0.80$ meV and $D_{Ni} = 0.54$ meV [29, 40]. T_N values for pure NiF_2 and FeF_2 samples were larger than expected from the bulk parameters, but this has been previously attributed to strain (piezomagnetism) [41, 42]. The exchange constants were therefore different than the bulk values ($J_{\mathrm{FeFe}} = 0.451$ meV and $J_{NiNi} = 1.72$ meV) [29, 40]. The non-monotonic dependence of T_2 on x is due to an enhancement of the exchange between unlike ions, $J_{\mathrm{FeNi}} = 0.88$ meV $> \sqrt{J_{\mathrm{FeFe}} J_{\mathrm{NiNi}}}$, similar to what has been observed in $Fe_xMn_{1-x}F_2$ [39]. It is unlikely that piezomagnetism could cause this effect because the strain should vary linearly between the $x = 0$ and $x = 1$ endpoints, given that FeF_2 and NiF_2 have the same crystal structure, which would lead to a monotonic dependence of T_2 on x.

MFT also predicts a region where oblique ordering occurs, similar to prior MFT results for

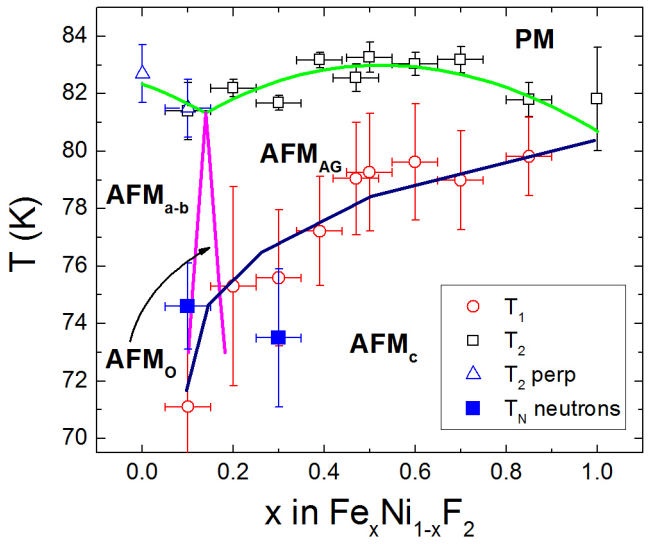

FIG. 4. $Fe_xNi_{1-x}F_2$ magnetic phase diagram. Regions are indicated by $AF_{a\text{-}b}$ (ordering in the a-b plane), AF_c (ordering along the c-axis), AF_{AG} (anisotropy glass phase), AF_O (oblique phase), and PM (paramagnetic phase). The PM-AF phase boundary calculated using MFT is denoted by the solid green curve. Horizontal error bars represent uncertainties from quartz crystal monitor measurements. Vertical error bars are transition widths σ_{T_C}. Measurements for samples that had a response for $H \perp$ to the c-axis ($[\bar{1}10]$ direction, $\triangle$) are also indicated. Magenta lines enclose the MFT AF_O region. Transitions observed via neutron scattering are indicated. The dark blue curve is a AF_c-AF_{AG} phase boundary drawn as a guide to the eye.

AF systems with anisotropic exchange couplings [16, 18]. The canting angle $\theta(T)$ calculated using our model is depicted in Fig. 3(c) [33]. The behavior was extremely sensitive to x. Remarkably good agreement was found for $x \sim 0.1205$, which is consistent with the sample's nominal concentration of $x = 0.1 \pm 0.05$, but with $J_{\mathrm{NiFe}} = 1.02$ meV. This indicates that other exchange interactions neglected by the model may play a role in determining $\theta(T)$. Although we cannot completely discount the possibility that AF order for the $x = 0.10$ sample is a result of local fluctuations in x that would locally tip the order from c-axis to $a-b$ plane ordering, the agreement of $\theta(T)$ data with theory suggests that the presence of the oblique phase is likely.

Regions of different types of order predicted by the calculations are indicated in Fig. 4. Whereas the calculated PM/AF boundary agrees well with T_2, neutron scattering data indicate that long-range order disappears for $T > T_1$. Therefore, a Griffiths-like [43–45]

short-range order phase exists in the $T_1 < T < T_2$ region as a result of the random single-ion anisotropy. Griffiths phases in AFs usually result from order parameter fluctuations reinforced by randomness in the exchange interactions. For example, magnetic field-induced antiferromagnetic fluctuations have been reported in metamagnetic $FeCl_2$ [46], in intraplanar frustrated $FeBr_2$[47], and in the dilute AFs $Fe_{1-x}Zn_xF_2$ [48] and $Rb_2Co_{1-x}Mg_xF_4$ [49]. Here we propose a mechanism where a breakdown of magnetic long-range order occurs at $T = T_1$ with the random orthogonal single-ion magnetic anisotropy playing the role of an effective local random field that enhances antiferromagnetic order parameter fluctuations. A RMA-induced anisotropy glass region exists in the interval $T_1 < T < T_2$, where T_2 is the upper phase transition determined by the average exchange interaction strength of the alloy.

In conclusion, the magnetic structure of $Fe_xNi_{1-x}F_2$, an authentic 3D AF with random single-ion magnetic anisotropy, transforms from easy a-b plane to the easy c-axis with increasing x via an oblique phase region at $x = 0.10-0.14$. Two phase transition temperatures, T_1 and T_2, were identified for $0.2 < x < 0.9$. Long-range order disappears for $T > T_1$, but short-range order persists up to $T = T_2$. The short-range order is a result of the RMA which induces a magnetic glass phase for $T_1 < T < T_2$. This phase is similar to magnetic glassy states formed as a result of combining structural disorder with frustrated exchange interactions, but with randomly distributed single-ion anisotropies replacing exchange frustration as the driving mechanism.

The support of the National Science Foundation (grant DMR-0903861), the WV Higher Education Policy Commission (RCG HEPC.dsr.12.29), and the Shared Research Facilities at WVU are gratefully acknowledged. Research conducted at ORNL and LANL was sponsored by the Scientific User Facilities Division, Office of Basic Energy Sciences, US Department of Energy. The Advanced Light Source is supported by the Director, Office of Science, Office of Basic Energy Sciences, of the U.S. Department of Energy under Contract No. DE-AC02-05CH11231.

---

* Current address: Integrated Microscopy Center, The University of Memphis, Memphis, TN 38152.

† david.lederman@mail.wvu.edu

[1] P. Miltényi, M. Gierlings, J. Keller, B. Beschoten, G. Güntherodt, U. Nowak, and K. D. Usadel, Phys. Rev. Lett. **84**, 4224 (2000).

[2] M. Cheon, Z. Liu, and D. Lederman, Appl. Phys. Lett. **90**, 012511 (2007).

[3] K. Kim, M.-S. Chang, S. Koernblit, R. Islam, E. E. Edwards, J. K. Freericks, G.-D. Lin, L.-M. Duan, and C. Monroe, Nature **465**, 590 (2010).

[4] T. Jörg, F. Krzakala, J. Kurchan, and A. C. Maggs, Progress of Theoretical Physics Supplement **184**, 290 (2010), http://ptps.oxfordjournals.org/content/184/290.full.pdf+html.

[5] D. Sherrington, Philosophical Transactions of the Royal Society A: Mathematical, Physical and Engineering Sciences **368**, 1175 (2010), http://rsta.royalsocietypublishing.org/content/368/1914/1175.full.pdf+html.

[6] G. E. Santoro, R. Martoňák, E. Tosatti, and R. Car, Science **295**, 2427 (2002), http://www.sciencemag.org/content/295/5564/2427.full.pdf.

[7] A. Srinivasan, Proceedings of the National Academy of Sciences **108**, 1751 (2011), http://www.pnas.org/content/108/5/1751.full.pdf+html.

[8] A. Barra and E. Agliari, Physica A: Statistical Mechanics and its Applications **391**, 3017 (2012).

[9] G. Facchetti, G. Iacono, and C. Altafini, Phys. Rev. E **86**, 036116 (2012).

[10] J. D. Bryngelson and P. G. Wolynes, Proceedings of the National Academy of Sciences **84**, 7524 (1987), http://www.pnas.org/content/84/21/7524.full.pdf+html.

[11] P. G. Wolynes, W. A. Eaton, and A. R. Fersht, Proceedings of the National Academy of Sciences **109**, 17770 (2012), http://www.pnas.org/content/109/44/17770.full.pdf+html.

[12] W. Zheng, N. P. Schafer, and P. G. Wolynes, Proceedings of the National Academy of Sciences **110**, 20515 (2013), http://www.pnas.org/content/110/51/20515.full.pdf+html.

[13] D. S. Fisher, G. M. Grinstein, and A. Khurana, Physics Today **41**, 56 (1988).

[14] P. Wong, P. M. Horn, R. J. Birgeneau, and G. Shirane, Phys. Rev. B **27**, 428 (1983).

[15] W.A.H.M. Vlak, E. Frikkee, A.F.M. Arts, and H.W. de Wijn, Phys. Rev. B **33**, 6470 (1986).

[16] F. Matsubara and S. Inawashiro, J. Phys. Soc. of Japan **42**, 1529 (1977).

[17] S. Fishman and A. Aharony, Phys. Rev. B **18**, 3507 (1978).

[18] F. Matsubara and S. Inawashiro, J. Phys. Soc. of Japan **46**, 1740 (1979).

[19] M. K. Wilkinson, J. W. Cable, E. O. Wollan, and W. C. Koehler, Phys. Rev. **113**, 497 (1959).

[20] T. Tawaraya and K. Katsumata, Solid State Commun. **32**, 337 (1979).

[21] T. Tawaraya, K. Katsumata, and H. Yoshizawa, J. Phys. Soc. Jpn. **49**, 1299 (1980).

[22] P. Z. Wong, P. M. Horn, R. J. Birgeneau, C. R. Safinya, and G. Shirane, Phys. Rev. Lett. **45**, 1974 (1980).

[23] K. Katsumata, J. Tuchendler, and S. Legrand, Phys. Rev. B **30**, 1377 (1984).

[24] Q. J. Harris, Q. Feng, Y. S. Lee, R. J. Birgeneau, and A. Ito, Phys. Rev. Lett. **78**, 346 (1997).

[25] D. P. Belanger and H. Yoshizawa, Phys. Rev. B **35**, 4823 (1987).

[26] A. Aharony, Phys. Rev. B **12**, 1038 (1975).

[27] K. Haefner, J. W. Stout, and C. S. Barrett, J. Appl. Phys. **37**, 449 (1966).

[28] W. Jauch, A. Palmer, and A. J. Schultz, Acta Cryst. B **49**, 984 (1993).

[29] M. T. Hutchings, M. F. Thorpe, R. J. Birgeneau, P. A. Fleury, and H. J. Guggenheim, Phys. Rev. B **2**, 1362 (1970).

[30] T. Moriya, Phys. Rev. **117**, 635 (1960).

[31] M. R. Fitzsimmons, D. Lederman, M. Cheon, H. Shi, J. Olamit, I. V. Roshchin, and I. K. Schuller, Phys. Rev. B **77**, 224406 (2008).

[32] M. Cheon, Z. Liu, and D. Lederman, J. Appl. Phys. **101**, 09E503 (2007).

[33] See Supplemental Material [url], which includes Refs. [50-61].

[34] R. J. Birgeneau, J. Magn. Magn. Mater. **177-181**, 1 (1998).

[35] D. Lederman, J. Nogués, and I. K. Schuller, Phys. Rev. B **56**, 2332 (1997).

[36] T. Tsushima, T. Teranishi, and K. Ohta, Handbook on magnetic substances (Asakura Publishing Co., Tokyo, 1975).

[37] D. Belanger and A. Young, J. Magn. Magn. Mater. **100**, 272 (1991).

[38] F. Ye, L. Zhou, S. Larochelle, L. Lu, D. P. Belanger, M. Greven, and D. Lederman, Phys. Rev. Lett. **89**, 157202 (2002).

[39] G. K. Wertheim, H. J. Guggenheim, M. Butler, and V. Jaccarino, Phys. Rev. **178**, 804 (1969).

[40] M. T. Hutchings, B. D. Rainford, and H. J. Guggenheim, J. Phys. C: Solid State Phys. **3**, 307 (1970).

[41] J. Mattsson, C. Djurberg, and P. Nordblad, J. Magn. Magn. Mater. **136**, L23 (1994).

[42] H. Shi, D. Lederman, K. V. O'Donovan, and J. A. Borchers, Phys. Rev. B **69**, 214416 (2004).

[43] R. B. Griffiths, Phys. Rev. Lett. **23**, 17 (1969).

[44] B. McCoy, Phys. Rev. Lett. **23**, 383 (1969).

[45] T. Vojta, J. Phys. A: Math. Gen. **39**, R143 (2006).

[46] C. Binek and W. Kleemann, Phys. Rev. Lett. **72**, 1287 (1994).

[47] C. Binek, M. de Azevedo, W. Kleemann, and D. Bertrand, J. Mag. Magn. Mater. **140–144**, 1555 (1995).

[48] C. Binek, S. Kuttler, and W. Kleemann, Phys. Rev. Lett. **75**, 2412 (1995).

[49] C. Binek, W. Kleemann, and D. P. Belanger, Phys. Rev. B **57**, 7791 (1998).

[50] H. Shi and D. Lederman, Phys. Rev. B **66**, 094426 (2002).

[51] H. Shi, Z. Liu, and D. Lederman, Phys. Rev. B **72**, 224417 (2005).

[52] M. Björck and G. Andersson, J. Appl. Cryst. **40**, 1174 (2007).

[53] H. Shi, D. Lederman, and E. E. Fullerton, J. Appl. Phys. **91**, 7763 (2002).

[54] A. P. Grosvenor, B. A. Kobe, M. C. Biesinger, and N. S. McIntyre, Surface and Interface Analysis **36**, 1564 (2004).

[55] J. Zaanen, C. Westra, and G. A. Sawatzky, Phys. Rev. B **33**, 8060 (1986).

[56] M. C. Biesinger, L. W. M. Lau, A. R. Gerson, and R. S. C. Smart, Phys. Chem. Chem. Phys. **14**, 2434 (2012).

[57] L. Yin, T. Tsang, and I. Adler, in Proc. Lunar Sci. Conf. 6th (Lunar and Planetary Institute, 1975) pp. 3277–3284.

[58] M. Hoppe, M. Gorgoi, C. Schneider, and M. Muller, Magnetics, IEEE Transactions on **50**, 1 (2014).

[59] G. K. Wertheim, S. Hüfner, and H. J. Guggenheim, Phys. Rev. B **7**, 556 (1973).

[60] F. de Groot, Journal of Electron Spectroscopy and Related Phenomena **67**, 529 (1994).

[61] O. Steinsvoll, R. M. Moon, W. C. Koehler, and C. G. Windsor, Phys. Rev. B **24**, 4031 (1981).